Nanofiber Composites of Polyvinyl Alcohol and Cellulose Nanocrystals: Manufacture and Characterization

Maria S. Peresin,[†] Youssef Habibi,[†] Justin O. Zoppe,[†] Joel J. Pawlak,[†] and Orlando J. Rojas*[,†,‡]

Department of Forest Biomaterials, North Carolina State University, Campus Box 8005, Raleigh, North Carolina 27695-8005, and Department of Forest Products Technology, Faculty of Chemistry and Materials Sciences, Helsinki University of Technology, P.O. Box 3320, FIN-02015 TKK, Espoo, Finland

Received November 4, 2009; Revised Manuscript Received December 24, 2009

Cellulose nanocrystals (CN) were used to reinforce nanofibers in composite mats produced via electrospinning of poly(vinyl alcohol) (PVA) with two different concentrations of acetyl groups. Ultrathin cross-sections of the obtained nanocomposites consisted of fibers with maximum diameters of about 290 nm for all the CN loads investigated (from 0 to 15% CN loading). The electrospinning process did not affect the structure of the PVA polymer matrix, but its degree of crystallinity increased significantly together with a slight increase in the corresponding melting temperature. These effects were explained as being the result of alignment and enhanced crystallization of PVA chains within the individual nanofibers that were subjected to high shear stresses during electrospinning. The strong interaction of the PVA matrix with the dispersed CN phase, mainly via hydrogen bonding or bond network, was reduced with the presence of acetyl groups in PVA. Most importantly, the elastic modulus of the nanocomposite mats increased significantly as a consequence of the reinforcing effect of CNs via the percolation network held by hydrogen bonds. However, this organization-driven crystallization was limited as observed by the reduction in the degree of crystallinity of the CN-loaded composite fibers. Finally, efficient stress transfer and strong interactions were demonstrated to occur between the reinforcing CN and the fully hydrolyzed PVA electrospun fibers.

Introduction

The development of micro/nanofibers has attracted significant interest in the last few decades due to the unique properties they endow, such as their very high surface area-to-volume ratio. This characteristic along with the remarkable suitability for surface functionalization and superior mechanical performance makes possible their use in a wide range of applications in medical, pharmaceutical, filtration, and catalysis fields, among others.[1,2] One of the possible routes for the production of micro/nanofibers is the electrospinning technique, which is based on the whipping of polymer solutions under electrostatic forces.[3−5]

Various polymers, including polyolefins, polyamides, polyesters, polyurethanes, polypeptides, and polysaccharides, have successfully been electrospun into micro- and nanofiber mats.[5] Poly(vinyl alcohol) (PVA), a commonly used polymer obtained by controlled hydrolysis of poly(vinyl acetate) (PVAc), can also be used to produce fibers via electrospinning. PVA is water-soluble, semicrystalline, fully biodegradable, nontoxic, and biocompatible, and therefore, it finds use in a broad spectrum of applications.[6] Furthermore, PVA-based fibers have been considered as an attractive choice in tissue scaffolding, filtration materials, membranes, optics, protective clothing, enzyme immobilization, drug release, and so on.[7]

Electrospun fibers produced from PVA have been extensively studied over the past few years with regard to the effects of production parameters,[8−11] molecular weight,[8,12,13] concentration,[14,15] solvent, and pH,[16] as well as the presence of additives.[17,18] Also, the mechanical and thermal properties, as well as the structural stability of PVA fibers, have been studied.[19,20]

A common feature of PVA fibers is their low mechanical strength and integrity, which have triggered alternatives such as post-treatment,[21] cross-linking,[14,22] and blending.[23,24] Furthermore, the use of nanofillers, such as carbon nanotubes,[25,26] inorganic nanoparticles based on hydroxyapatite,[27] gold,[28] silver,[29] clay,[30−32] silica,[33] cellulose nanofibrils,[34] and chitin whiskers,[35] have been reported.

Currently, numerous efforts are focused on the use of materials from renewable resources as reinforcement agents in nanocomposites. Among such materials readily available, cellulose nanocrystals (CNs) have attracted great interest due to their renewability, biodegradability, and spectacular mechanical properties. As such, we have reported on the use of CNs to reinforce polymer matrices in electrospun composite mats consisting of poly(caprolactone)[36] and polystyrene.[37] In this work, we describe the manufacture of electrospun materials based on PVA mats reinforced with CNs. The morphology of the resulting fibers was analyzed by transmission electron microscopy (TEM) and scanning electron microscopy (SEM). Finally, the enhancement of the thermomechanical properties of electrospun PVA nonwoven mats was demonstrated by thermal gravimetric analysis (TGA), differential scanning calorimetry (DSC), and dynamic mechanical analysis (DMA).

Materials and Methods

Polymer Matrix. Two PVAs were used, both with approximately the same molecular weight but different residual acetyl content of 2 and 12%. The acetyl groups were originated from the precursor vinyl acetate that was subject to hydrolysis to produce PVA. The corre-

* To whom correspondence should be addressed. E-mail: ojrojas@ncsu.edu.
[†] North Carolina State University.
[‡] Helsinki University of Technology.

10.1021/bm901254n
Published on Web 01/20/2010

Table 1. Main Characteristics of the PVA Polymers Used in this Work

PVA trade name	abbreviated name	average M_w (Da)	nominal percent of acetyl groups (%)
Mowiol 20−98	PVA-98	125000	2
Mowiol 40−88	PVA-88	127000	12

Table 2. Physical Properties of Suspensions of PVA and PVA Loaded with CNs Used in Electrospinning[a]

polymer	CNs content in PVA/CN suspensions (%)	surface tension (mN/m)	viscosity ($\times 10^{-2}$ Pa·s)	conductivity (μS/cm)
PVA-98	0	62.5 ± 0.3	15.1 ± 0.1	17.6 ± 0.4
	5	62.6 ± 0.2	18.1 ± 0.5	23.3 ± 0.3
	10	62.1 ± 0.8	17.2 ± 0.1	29.4 ± 0.6
	15	62.6 ± 0.1	17.8 ± 0.2	36.7 ± 0.5
PVA-88	0	50.4 ± 0.3	39.1 ± 0.1	129.1 ± 0.2
	5	50.8 ± 0.1	39.0 ± 0.2	129.2 ± 0.1
	10	51.1 ± 0.4	40.8 ± 0.4	139.0 ± 0.3
	15	51.4 ± 0.1	39.7 ± 0.2	142.9 ± 0.5

[a] The errors in surface tension, viscosity, and conductivity were calculated from the standard deviation in triplicate measurements.

sponding degrees of hydrolysis were 98 and 88% for fully and partially hydrolyzed polyvinyl acetate, respectively. Thereafter, they will be referred to as PVA-98 and PVA-88 to indicate the respective hydrolysis degree. These polymers were purchased from Sigma-Aldrich and Fluka, respectively. Their trade name and main characteristics are included in Table 1.

Cellulose Nanocrystals (CNs). The CNs were obtained by acid hydrolysis of pure ramie fibers (Stucken Melchers GmbH & Co., Germany) as described elsewhere.[38] Briefly, the fibers were extracted with 4 wt % aqueous NaOH solution during 2 h at 80 °C to remove residual additives. They were then hydrolyzed with 65 wt % sulfuric acid at 55 °C for 45 min under vigorous mechanical stirring. The resulting suspension was cooled in an ice bath and filtered through a No. 1 glass sinter to remove unhydrolyzed material and finally washed with deionized water by successive centrifugations (12000 rpm at 10 °C for 20 min) until neutral pH. Dialysis against deionized water was performed for 7 days to remove free acid molecules from the suspension. Finally, the suspension was sonicated and a few drops of chloroform were added to avoid degradation. The suspension was kept refrigerated until use. The concentration of CNs in the final dispersion was determined gravimetrically.

Preparation of PVA-CN Suspension. Aqueous solutions of PVA-98 and PVA-88 were prepared and the corresponding amounts of CN dispersions (see above) were added to obtain a final nanocrystal content of 0, 5, 10, and 15% (w/w), while keeping total PVA concentrations constant at 7%. The resulting suspensions were kept under vigorous mechanical stirring at 80 °C for 120 min, at the end of which cooling was allowed under same vigorous stirring until the system reached room temperature. The mixtures were stored in the refrigerator; any given batch was stored for no longer than 1 week prior to its use. The viscosity, conductivity, and surface tension of the respective suspensions were determined at 25 °C by a programmable rheometer (AR2000, TA Instruments), conductivity meter (Corning Inc., model 441), and a du Noüy Ring tensiometer (Fisher tensiomat, model 21), respectively (see Table 2 in Results and Discussion).

Electrospinning. Fibers from PVA suspensions (with or without CN added) were obtained by horizontal electrospinning. The electrospinning setup included 10 mL plastic, disposable syringes with 22-G needles connected to the positive terminal. Polymer solution flow was controlled with a syringe pump (Aldrich) that was regulated with a Pump-term code. The high-voltage supply unit (Series EL, Glassman High Voltage) had a power range of 0−50 DC kV. A 30 cm diameter plate covered by aluminum foil and connected to the negative electrode of the power supply (ground) was used as collector. The needle tip-to-collector or working distance was 15 cm.

Conditioning of the Electrospun Mats. The collected electrospun fiber mats were kept in an oven at 40 °C under vacuum to remove any residual water. Whenever the samples were taken out of the oven for analysis, they were maintained in a desiccator containing P_2O_5 to ensure a moisture-free environment. Equilibrium moisture content in the fiber mats was reached after this conditioning and confirmed by weighing the samples and noting that, after 180 min, no significant mass changes occurred.

Scanning Electron Microscopy (SEM). The morphology of the nanofibers in the electrospun mats was checked using field emission scanning electron microscopy (FE-SEM) using a JEOL 6400F microscope operated with an accelerating voltage of 5 kV and a working distance of 20 mm. A small portion of the nanofiber mat was fixed on conductive carbon tape and mounted on the support and then sputtered with an approximately 6 nm layer of gold/palladium (Au/Pd). Under the same conditions, the cross-sections of the nanofiber mats were analyzed, applying a cryogenic protocol before coating. In additional experiments, ultrathin cross-sections of the samples were obtained. To this end, a Cross Section Polisher (JEOL, Peabody, MA) operating with an argon Beam Milling (5 kV Ar^+ ion beam) was used to section the samples after they were fixed between thin copper tapes. Coating with a thin layer of carbon followed before analysis with a thermal JEOL JSM-7600F FEG-SEM operated at variable pressure and low voltage, while still maintaining high resolution. The diameter and diameter distribution of the fibers in the mats were determined by using the UTHSCSA Image Tool for Windows version 3.0 with sample sizes of at least 250 fibers per SEM micrograph. Statistical analysis was performed using OriginPro 8, one-way analysis of variance (ANOVA).

Transmission Electron Microscopy (TEM). For CN imaging with TEM, a few drops of aqueous CN suspension (0.01% w/v) were deposited on carbon-coated electron microscope grids, negatively stained with uranyl acetate and then allowed to dry. The grids were observed with a Hitachi HF2000 TEM operated at an accelerating voltage of 80 kV.

Fourier Transform Infrared Spectroscopy (FTIR). FTIR was used to chemically confirm the presence of the CNs inside the matrices of PVA nanofibers. The electrospun mats of PVA and CN-loaded PVA were dried overnight in an oven at 40 °C under vacuum and then directly analyzed in a Nicolet FTIR spectrometer. All spectra were collected with a 2 cm^{-1} wavenumber resolution after 64 continuous scans.

Thermal Gravimetric Analysis (TGA). Thermogravimetric analyses were performed using a TA Instruments TGA Q500. In a typical experiment, between 10 and 20 mg of sample were placed in a clean platinum pan and heated from 30 to 600 °C at a rate of 10 °C/min.

Differential Scanning Calorimetry (DSC). Differential scanning calorimetry was carried out with a TA Instruments DSC Q100. The typical procedure included heating of approximately 10 mg of sample in a DSC pan from −50 to 250 °C using a heating rate of 10 °C/min.

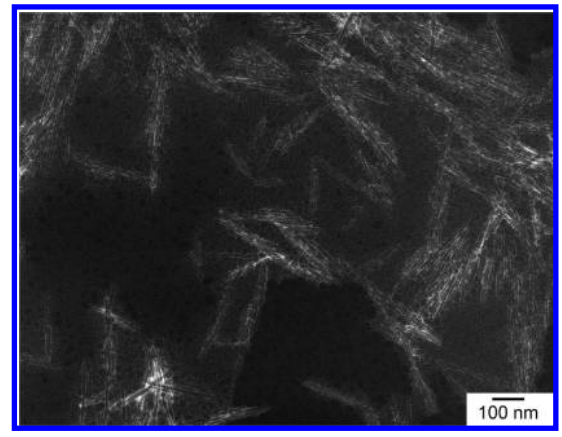

Figure 1. TEM micrograph of cellulose nanocrystals from ramie fibers.

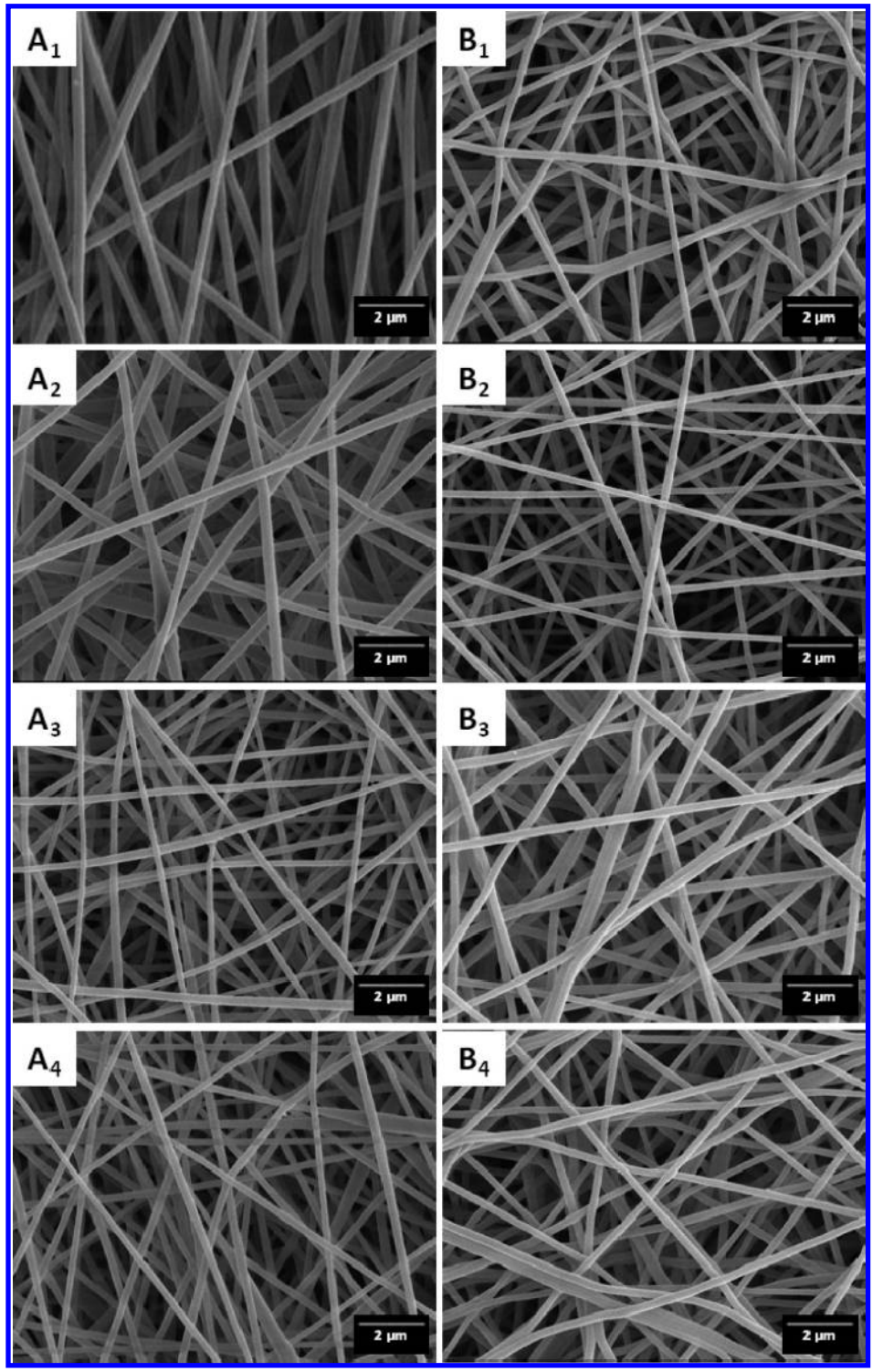

Figure 2. Representative scanning electron micrographs of electrospun fibers based on fully hydrolyzed PVA-98 (A_{1-4}) and partially acetylated PVA-88 (B_{1-4}) loaded with cellulose nanocrystals (the subscripts 1, 2, 3, and 4 are used to indicate CN loadings of 0, 5, 10, and 15 wt %, respectively).

In tests with DSC the melting temperature (T_m) was taken as the onset temperature of the melting endotherms of the sample. To obtain the degree of crystallinity, the samples were heated at a rate of 10 °C/min and maintained at 100 °C for 5 min and then cooled down to 0 °C using a cooling rate of 10 °C. The peak of the crystallization exotherm was taken as the crystallization temperature (T_c) of the sample.

Dynamic Mechanical Analysis (DMA). Dynamic mechanical analysis was performed in tensile mode (TA Instruments Q800). The measurements were carried out with 6 mm sample strips cut out of the corresponding electrospun mats using a gap between jaws of 10 mm. DMA tests used a constant frequency of 1 Hz, strain amplitude of 0.03%, and a temperature range of −100−250 °C (heating rate of 3 °C/min).

Results and Discussion

CNs extracted from ramie fibers by sulfuric acid-catalyzed hydrolysis are shown in the TEM micrograph shown in Figure 1. Some bundles of cellulose nanocrystals were observed,

however, individual CNs were easily distinguished as being rod-like in shape, 3−10 nm in width (*w*), and 100 and 250 nm in length (*L*). The aspect ratio, that is, the length to width ratio *L*/*w*, was calculated to be around 27.

Uniform spinning or ejection of the charged jet required the concentration, viscosity, conductivity, and surface tension of the polymer solution to be optimized. Therefore, prior to electrospinning, the different systems used to produce electrospun mats were characterized in terms of the above properties (see Table 2). Neither the surface tension nor the viscosity of the suspensions was significantly affected by the addition of CNs for both types of PVA polymers. However, the conductivity increased with addition of CNs as a result of the negative charges from the sulfate ester groups on their surfaces. These sulfate groups were grafted on the surface of CNs during production via acid hydrolysis catalyzed with sulfuric acid. Their amount was estimated by elemental analysis to be around 0.7%, which according to the surface area of the CN nanoparticles corresponded to a surface charge of about 0.30 e/nm^2.[39] The increase in suspension conductivity was significant in the case of suspensions of CN-loaded PVA-98 because it increased up to more than double the value corresponding to CN-free PVA-98 (36 compared to 17 μS/cm). In contrast to PVA-98, in the case of PVA-88 polymer, the increase in conductivity was limited to 10%. Moreover, the conductivity for the PVA-88 suspensions was much higher than that for PVA-98 ones. This could be related to the presence of residual electrolytes as impurities in the commercial PVA-88 sample. The PVA-88 solutions presented higher viscosities compared to those from PVA-98; in all cases, the addition of CNX did not produce significant changes in viscosities.

The operational conditions were carefully examined by performing a series of electrospinning runs at different electric field strengths, polymer concentration in the electrospinning solution, and flow rates. Suitable conditions for electrospinning PVA, with or without added CN, included 10 kV with a tip-to-collector distance of 15 cm (equivalent to a strength of electric field of 0.67 kV/cm) and flow rate of 0.48 mL/h. The electric field strength was somewhat smaller compared to the conditions reported in the literature of 1−2 kV/cm for neat PVA of relatively the same characteristics. All results reported later corresponded to electrospun fiber mats produced from suspensions that were processed under the electrospinning conditions stated above and operating at room humidity and temperature.

Morphological and Chemical Characterization of CN-Loaded PVA Nanofiber Mats. The morphology of fibers in the mats produced by electrospinning, under the conditions previously presented, was studied by SEM. Figure 2 shows typical SEM micrographs for fibers electrospun from neat PVA and also from PVA with different CN concentrations (5, 10, and 15%). All polymer compositions considered yielded uniform and smooth, bead-free nanofibers. In the case of fully hydrolyzed PVA (PVA-98), individualized fibers were observed (see Figure 2A_1 and A_2), which is in contrast to the case of fibers obtained from acetylated PVA (PVA-88) that formed some few fiber doublets or fibers partially fused together (see Figure 2B_1 and B_2). The average diameters of the fibers based on neat PVA-98 and PVA-88 were around 235 and 275 nm, respectively (see Table 3).

Even though some variation in diameters was observed, depending on the amount of CNs present in the fibers, the largest average diameter determined was about 290 nm. For fibers based on PVA-98, the addition of CN induced a significant reduction in the diameter of the electrospun fibers down to 188 nm (95% confidence level) in the case of 15% CN content. The change in the ionic strength and conductivity of the electrospinning solution (see Table 1) produced by the negatively charged CNs was believed to be the main contribution to this fiber diameter reduction. This is explained by the fact that an increased electrostatic charge density of the electrospinning solution induced more extensive filament stretching during jet whipping. In contrast to the case of PV-98, addition of CNs to PVA-88 produced no clear effect in the diameter of the respective electrospun fibers. Also, it was observed that the statistical size distribution in this case was not normal.

Table 3. Average Diameters and Standard Deviation of Electrospun Fibers Based on PVA-98 and PVA-88

polymer	CN content (%)	diameter (nm)	standard deviation (nm)
PVA-98	0	235	64
	5	245	58
	10	182	51
	15	188	41
PVA-88	0	274	54
	5	293	78
	10	268	37
	15	295	83

Visualization of CNs inside the electrospun fibers proved to be a challenge with standard TEM methods, likely because the lack of contrast between the two organic components, PVA and CN, even after addition of uranyl acetate staining agent to the dispersion before electrospinning or after use of high TEM magnification. Therefore, cryo-SEM and FE-SEM of ultrathin cross-sections (after polishing with 5 kV Ar^+ ion beam) of the electrospun mats were carried out for more detailed morphological analysis.

It is worth noting that cast films from CN-filled PVA were reported to have small, bright features in SEM cross-sections, which were attributed to the CNs present.[40−42] As such, Figure 3 shows representative images obtained for PVA-98-based nanofibers containing 15% of CNs. Cryo-SEM (Figure 3A_1 and A_2) and variable pressure, ultrahigh resolution FE-SEM micrographs in transversal cross-sections (Figure 3B_1 and B_2) of ultrathin fiber mats. Figure 3A_2 indicates internal features likely related to the presence of CNs, as was indicated above in the case of cast films. In Figure 3B_1 and B_2, the cross-section allowed examination of the high porosity of the mats. In Figure 3B_2, the carbon coating used to achieve high resolution imaging masked the internal features of the fibers that were otherwise observed in Figure 3A_2.

To confirm the presence of CNs in the PVA nanofiber mats, they were subjected to analysis with Fourier-transform infrared spectroscopy (FTIR). As such, collected spectra for both types of PVA polymers, neat and loaded with 15% of CNs, are presented in Figure 4. All major peaks related to hydroxyl and acetate groups were evident in the spectra corresponding to the neat PVA: The large bands observed between 3550 and 3200 cm^{-1} were typical of the stretching O−H from the intermolecular and intramolecular hydrogen bonds. The presence of acetyl groups within the PVA-88 polymer disrupted this hydrogen bond network and therefore resulted in a change of the shape of this characteristic peak. The vibrational band observed between 2840 and 3000 cm^{-1} corresponded to the stretching C−H from alkyl groups, and the peaks between 1750−1735 cm^{-1} were assigned to the C═O and C−O stretching from residual acetate groups in the PVA matrix. The intensity of the later peak was small in the case of PVA fibers with low acetyl content, PVA-98 (2% acetyl group concentration), while a very strong peak for PVA-88 (12% acetyl group

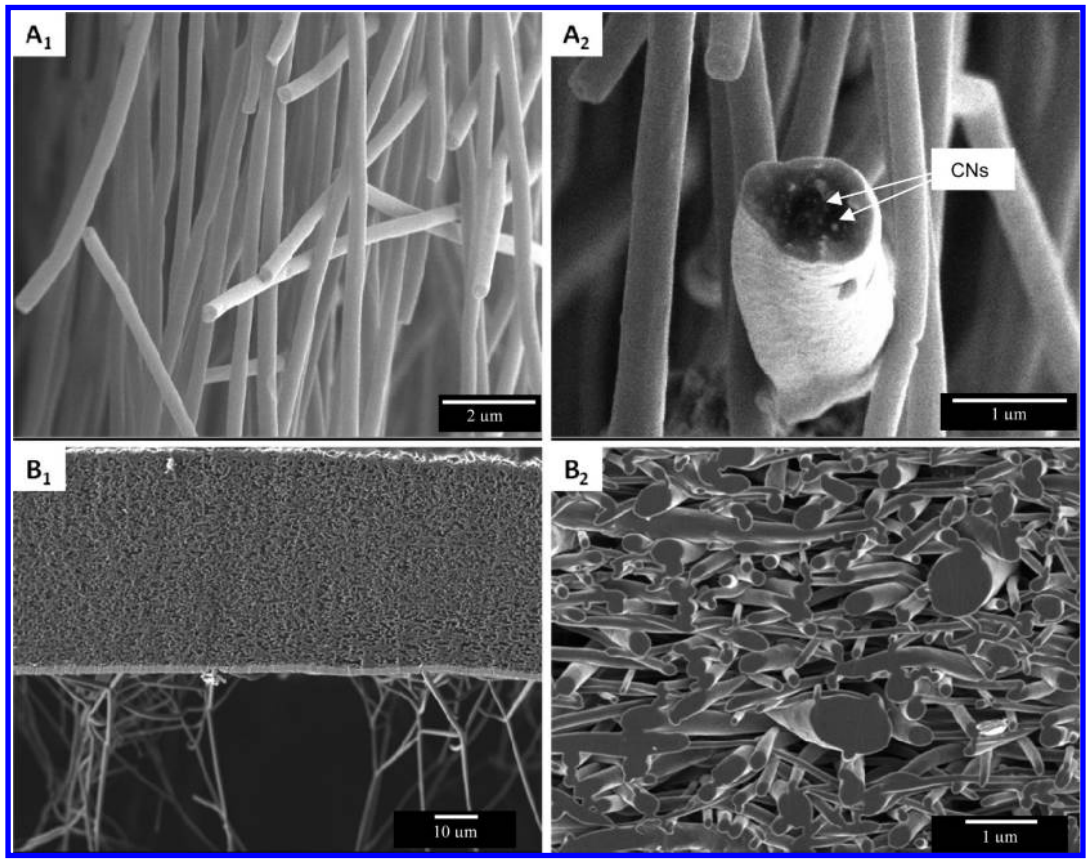

Figure 3. Cryo-SEM (A_1 and A_2) and variable pressure, ultrahigh resolution FE-SEM micrographs in transversal cross-sections (B_1 and B_2) of electrospun PVA-98 loaded with 15% of CNs. The top and bottom, bright thin layers observed in B_1 are from a copper tape used to protect the sample and to facilitate cross-section by 5 kV Ar^+ ion polishing. The straggling fibers (ca. 1 μm diameter) in the same image are not related to the PVA fiber mat. Bar sizes in each image are as follow: $A_1 = 2$ μm, $A_2 = 1$ μm, $B_1 = 10$ μm, and $B_2 = 1$ μm.

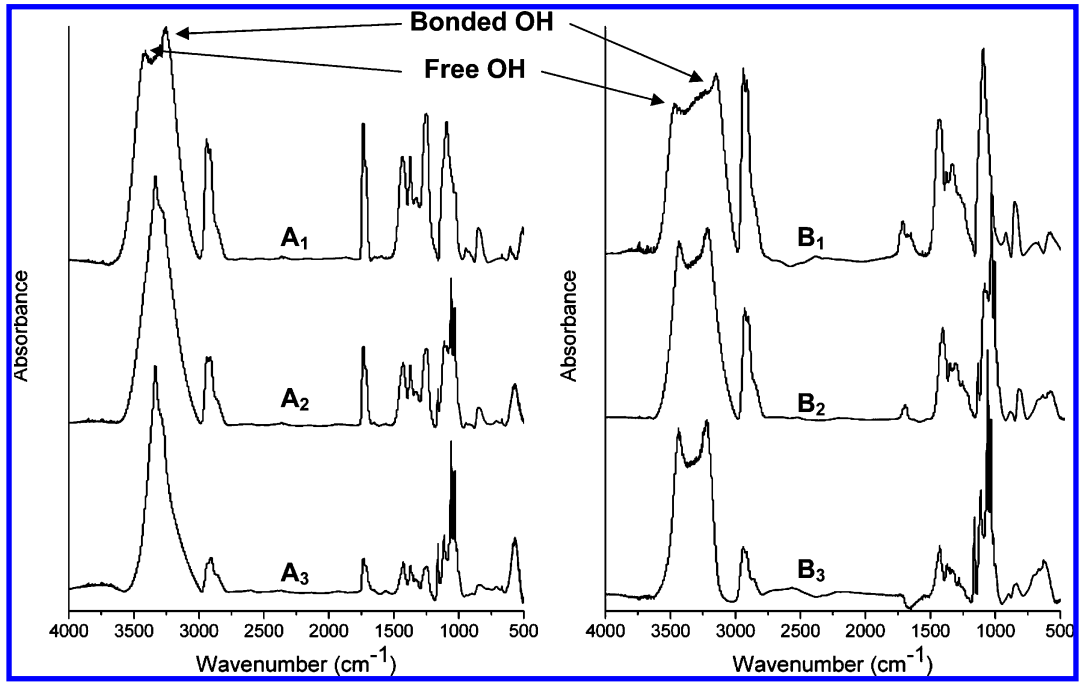

Figure 4. FTIR spectra corresponding to electrospun fibers of PVA-98 (A) and PVA-88 (B) with different loadings of CNs: 0 and 15 wt % (subscripts "1" and "2", respectively). The spectra indicated by subscript "3" were obtained after subtraction of the PVA spectra ("1") from the respective composite spectra ("2").

concentration) indicated the presence of acetate groups in the polymer chain.

For both CN-filled PVA-88 and CN-filled PVA-98, the FTIR spectra showed the typical bands corresponding to the matrix polymer; most importantly, the presence of CNs produced distinctive changes in the shape and intensity of the main peaks. This is explained by the strong interactions present, mainly due to hydrogen bonding or bond network between the hydrophilic

CN reinforcement nanoparticles and the PVA continuous polymer matrix. Support for this explanation is provided by the band observed between 3550 and 3200 cm^{-1}, which is characteristic of the stretching O−H from the intermolecular and intramolecular hydrogen bonds. The shape of this band was substantially different when comparing the neat and the CN-filled PVA.

The presence of CNs in the nanocomposites was confirmed by subtracting the PVA spectrum from that of the respective composite and comparing the obtained spectrum with that of pure cellulose. A scale factor was used in this spectral subtraction to ensure that the absorption band of PVA (at 850 cm^{-1}), which does not overlap with any band for cellulose, was canceled out. For all CN loadings, the resulting subtraction spectra were very similar, quite reproducible, and followed closely the typical spectrum of cellulose, with all its characteristic bands present. However, FTIR peak shapes and relative intensities were noted to differ somewhat from that of reference cellulose, which can be ascribed to new intermolecular interactions in the composites, mainly due to hydrogen bonding with PVA macromolecule in the electrospun fibers. Similar observations have been reported in the case of blends of PVA with chitin[43] or chitosan.[44]

According to the subtracted spectra, the most relevant feature is the existence of a 3600−3000 cm^{-1} band which is related to OH group stretching vibrations. Comparison of these bands for the composites with PVA-98 and PVA-88 indicated a difference in their shape that depended on the acetyl content, which, in turn, produced significant differences in the interaction between the two components of the composite fibers. Such interaction was expected and indeed observed (via FTIR spectra) to be strongest for the PVA-98-CN system.

Thermal Properties of the PVA-CN Nanofiber Composites. Thermogravimetric analysis (TGA) and differential scanning calorimetry (DSC) were used to investigate the effect of CN on the thermal stability of the composites and also to obtain deeper insights on the interactions between the dispersed and continuous phases of the nanofibers. The stability of PVA polymer during the electrospinning process was investigated by comparing samples of bulk, "as-received" PVA with electrospun PVA. The corresponding TGA thermograms of the first-order derivatives, revealing the temperatures at which the maximum weight losses occurred, are shown in Figure 5 for both fully hydrolyzed PVA (PVA-98, Figure $5A_{1,2}$) and partially hydrolyzed PVA (PVA-88, Figure $5B_{1,2}$). It can be observed that the difference in the TGA's first-order derivative before and after electrospinning was negligible; therefore, it is concluded that the electrospinning process did not affect the structure of the matrix polymer.

The thermograms of PVA-98 showed two regions with a temperature for maximum mass loss at around 375 and 440 °C, which corresponded to the chain-stripping produced by the removal of water molecules (dehydration of the PVA polymer) followed by chain scission and decomposition.[45] For partially acetylated PVA, PVA-88, the first region corresponding to the removal of water shifted toward lower temperatures and the corresponding peak separated into two peaks. The first peak, at the maximum temperature of about 323 °C, can be related to the release of the acetyl groups that were transformed to acetic acid molecules and consequently catalyzed by in situ chain-stripping. Interestingly, this phenomenon took place at lower temperatures when compared to the case of fully hydrolyzed PVA, PVA-98. However, when comparing PV-88 and PV-98, it was observed that the temperature ascribed to the chain decomposition peak remained unaffected.

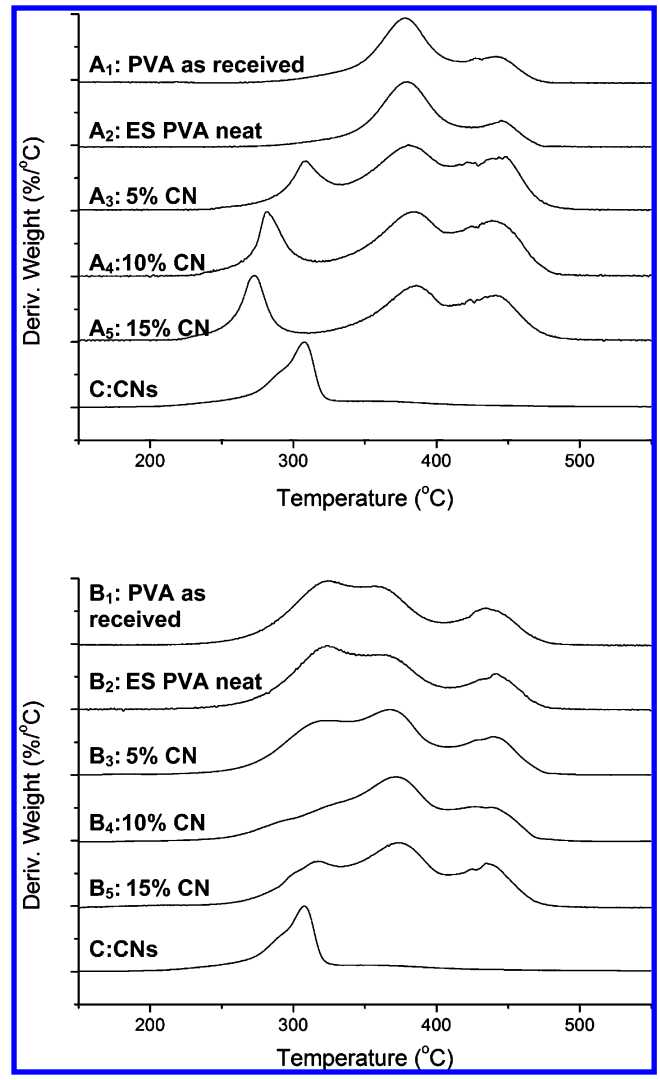

Figure 5. Thermograms of PVA-98 (A_{1-5}) and PVA-88 (B_{1-5}). Profiles from top to bottom correspond to as-received PVA polymer (subscript 1), neat PVA electrospun (ES) mats (subscript 2), and electrospun PVA loaded with CN at various wt %: 5 (subscript 3), 10 (subscript 4), and 15 (subscript 5) wt %. Thermograms for pure CNs are added as a reference (C).

After addition of 5% CN into PVA-98, a new peak at about 300 °C appeared in the electrospun nanofibers, as can be seen in the first-order derivative curve. This can be explained by the degradation of CNs, as can be confirmed in the thermogram of pure CN added as reference in Figure 5C. As the CN loading was increased to 15%, this peak shifted to lower temperatures (273.1 °C). The observed shift in degradation temperature can be explained by the high temperature decomposition of CNs accelerated in PVA melt polymer, due to differences in solid state properties, and also from possible degradation catalyzed by residual acetic acid via ester pyrolysis.[46] In the case of nanofibers from PVA-88, no clear shift in CNs thermal decomposition was observed even when used at the highest CN loadings of 15%. This fact provides additional evidence as to the interactions and ensuing thermal degradation temperatures, between the two types of PVA polymers and the reinforcing CN, depending on the extent of interaction (interfacial adhesion) between the continuous and the dispersed phases.

Differential scanning calorimetric analyses were carried out on both PVA polymers, before and after electrospinning, as well

Table 4. Effect of Electrospinning and CN Loading on the Melting Temperature (T_m) and Degree of Crystallinity (χ_c) of Composite Nanofibers[a]

sample	CN content (wt%)	T_m (°C)	ΔH_m (J/g)	χ_c
PVA-98, as received	0	220.7	79.0	0.50
PVA-98, electrospun	0	222.8	111.3	0.70
	5	222.6	106.3	0.70
	10	221.5	80.4	0.56
	15	221.1	72.8	0.54
PVA-88, as received	0	191.7	43.9	0.32
PVA-88, electrospun	0	193.7	56.1	0.40
	5	193.3	60.0	0.45
	10	193.7	37.4	0.30
	15	193.5	50.3	0.42

[a] $\chi_c = (\Delta H_m)/((\Delta H_m^0 \times \omega))$, with ΔH_m^0 is the heat of fusion for the 100% crystalline polymer, which is estimated to $\Delta H_m^0 = 158$ J/g for PVA-98 and $\Delta H_m^0 = 139$ J/g for PVA-88;[48] w is the weight fraction of polymeric material in the respective composite; AR = as received PVA; and ES = electrospun mats from PVA or PVA-CN systems.

as after adding CNs at different loadings. Table 4 indicates the measured melting temperature and degree of crystallinity for all materials studied. It was observed that after electrospinning the degree of crystallinity of both PVA neat polymers increased significantly. The corresponding melting temperature also increased slightly, by about 2 °C, for each PVA polymer. These effects are explained as the result of alignment and enhanced crystallization of the polymer chains within the individual PVA fibers that were subjected to very high shear stresses during electrospinning. However, this organization-driven crystallization was undermined upon addition of CNs because the degree of crystallinity decreased in the composite nanofibers. Disorder and decrease of PVA nucleation in the presence of CNs may have taken place during the short time allowed during electrospinning. In fact, such nucleating effect has been reported in the case of CN-filled PVA solid film produced by casting-evaporation technique.[47] On the other hand, the melting temperature T_m of electrospun fibers containing CN at different loadings remained fairly constant for both sets of the PVA samples.

Mechanical Properties of PVA-CN Nanofiber Composites. To evaluate the mechanical properties of nanofiber mats obtained after electrospinning of PVA polymers and the corresponding nanocomposites with CN, longer electrospinning collection times were used to produce thicker mats suitable for DMA analyses. The mechanical analyses were performed by DMA in linear tensile mode, and the main results are presented in Figure 6.

All composites based on the partially hydrolyzed PVA-88 displayed the typical behavior of amorphous polymers due to the low degree of crystallinity (see Table 4). In the glassy state, the modulus remained roughly constant; by increasing the temperature, a sharp drop in the storage modulus occurred at around 80 °C, which corresponded to the primary relaxation process, glass−rubber transition. This drop in the storage modulus can be ascribed to an energy dissipation phenomenon involving cooperative motions of the polymer chains. Meanwhile, the value of the storage modulus decreased with temperature due to irreversible polymeric chain flow and disentanglement that are typical in amorphous polymers. At higher temperatures, DMA measurements were no longer possible, as expected.

In contrast to the electrospun nanofiber mats based on PVA-88, the storage modulus of all CN-loaded PVA-98 nanocomposites displayed the typical behavior of partially crystalline polymers, with their three distinctive zones. At low temperature (below 80 °C), the modulus decreased very slightly with

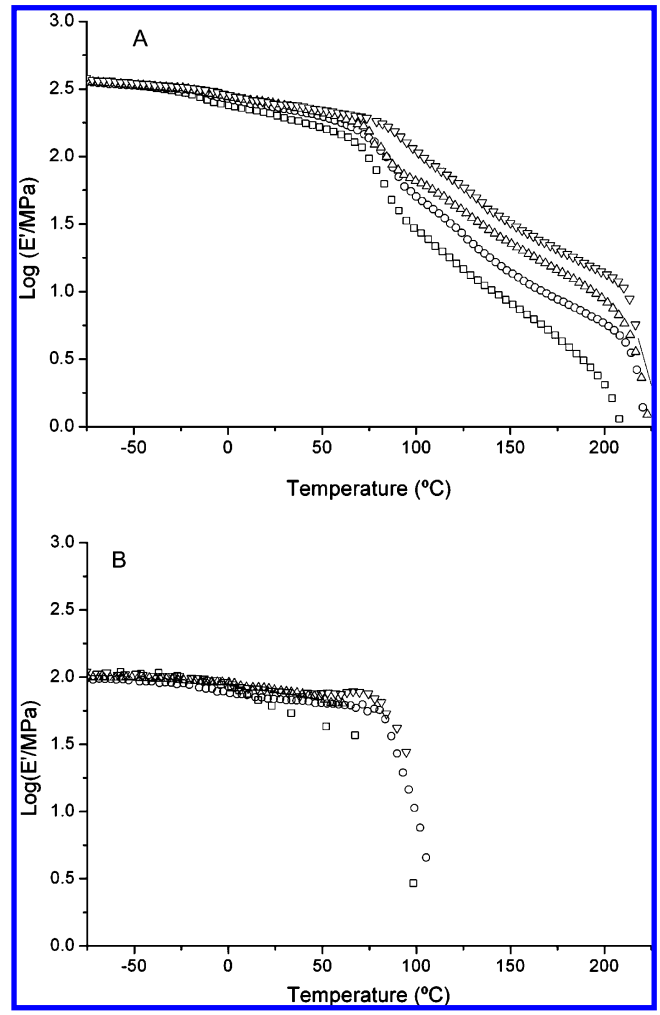

Figure 6. Storage modulus of electrospun nanfiber mats vs temperature for fully hydrolyzed PVA-98 (A) and partially hydrolyzed PVA-88 (B) with different loadings of cellulose nanocrystals (□ 0%, ○ 5%, Δ 10%, and ▽ 15%).

temperature, as expected for a glassy state. At approximately 80 °C, a transition that appeared as a drop in the storage modulus was due to the main relaxation process. At a temperature range between 80 to approximately 200 °C, the amorphous, rubbery, and crystalline domains coexisted and the storage tensile modulus decreased due to the progressive flow of the amorphous component and also due to the melting of the crystalline part of the PVA-98 matrix. At even higher temperatures (above 200 °C), the modulus dropped sharply due to unrecoverable deformations in the completely melted PVA-98 polymer matrix.

An additional important feature was observed in that the modulus of the nanocomposite mats increased significantly upon CN loading in PVA-98. Because a decrease in the crystallinity (see Table 4) would be expected to induce a reduction in the storage modulus, it is therefore concluded that the observed strength enhancement in CN-loaded PVA mats can only be related to the reinforcing effect of the dispersed phase, via the percolation network held by hydrogen bonds. The values of the storage moduli at 125 °C extracted from the DMA curves of PVA-98 composite mats are reported in Table 5. The enhancement in mechanical strength was estimated to be more than 3-fold when composites with 15% CN loading are compared to the respective neat PVA. These results demonstrate efficient stress transfer between CN and PVA-98 polymer in the electrospun fibers. All these observations corroborate the

Table 5. Storage Modulus (E') of Electrospun PVA-98 Fiber Mats with Different Loadings of Cellulose Nanocrystals Measured at 125 °C

CNs content (%)	E' (MPa)
0	15.45
5	25.76
10	38.20
15	57.30

existence of strong interactions between the reinforcing CN phase and the fully hydrolyzed PVA-98 continuous phase.

Conclusions

Fiber nanocomposites of PVA reinforced with cellulose nanocrystals were successfully produced by the electrospinning technique. Very smooth nonwoven mats with homogeneous nanofibers were obtained, showing enhanced thermomechanical properties as a result of the addition of cellulose nanocrystals to the PVA polymer matrix. Reinforcing cellulose nanocrystals induced a 3-fold increase of the storage modulus of fully hydrolyzed PVA, which was ascribed to the efficient stress transfer between CN and PVA polymer in the electrospun fibers. In contrast, this effect was not observed for the partially hydrolyzed PVA. This observation was explained by differences in hydrogen bond network in the respective systems, as revealed by infrared spectroscopy. Overall, the existence of strong interactions between the reinforcing CN phase and the fully hydrolyzed PVA continuous phase was demonstrated.

Acknowledgment. The authors acknowledge financial support from the National Research Initiative of the USDA Cooperative State Research, Education and Extension Service, Grant Nos. 2007-35504-18290 and 2008-35504-19203. We also gratefully acknowledge Regina Campbell and Patricia Corkum (JEOL Inc., U.S.A.) for assistance with experiments with the cross-section polisher.

References and Notes

(1) Kotek, R. *Polym. Rev.* **2008**, *48*, 221–229.
(2) Burger, C.; Hsiao, B. S.; Chu, B. *Annu. Rev. Mater. Res.* **2006**, 333–368.
(3) Huang, Z.-M.; Zhang, Y.-Z.; Kotaki, M.; Ramakrishna, S. *Compos. Sci. Technol.* **2003**, *63*, 2223–2253.
(4) Greiner, A.; Wendorff, J. *Angew. Chem., Int. Ed.* **2007**, *46*, 5670–5703.
(5) Frenot, A.; Chronakis, I. S. *Curr. Opin. Colloid Interface Sci.* **2003**, *8*, 64–75.
(6) Finch, C. A. *Polyvinyl alcohol; properties and applications*; Wiley Interscience: New York, 1973.
(7) Nishiyama, M. *Chem. Fibers Int.* **1997**, *47*, 296–297.
(8) Lee, H. W.; Karim, M. R.; Park, J. H.; Bae, D. G.; Oh, W.; Cheong, I. W.; Yeum, J. H. *Polym. Polym. Compos.* **2009**, *17*, 47–54.
(9) Erika Adomaviciute, R. M. *Fibres Text. East. Eur.* **2007**, *15*, 69–72.
(10) Kong, C.-S.; Lee, T.-H.; Lee, K.-H.; Kim, H.-S. *J. Macromol. Sci. B* **2009**, *48*, 77–91.
(11) Zhang, C.; Yuan, X.; Wu, L.; Han, Y.; Sheng, J. *Eur. Polym. J.* **2005**, *41*, 423–432.
(12) Koski, A.; Yim, K.; Shivkumar, S. *Mater. Lett.* **2003**, *58*, 493–497.
(13) Joon Seok Lee, K. H. C.; Ghim, H. D.; Kim, S. S.; Chun, D. H.; Kim, H. Y.; Lyoo, W. S. *J. Appl. Polym. Sci.* **2004**, *93*, 1638–1646.
(14) Ding, B.; Kim, H.-Y.; Lee, S.-C.; Lee, D.-R.; Choi, K.-J. *Fibers Polym.* **2002**, *3*, 73–79.
(15) Jia, Z.; Li, Q.; Liu, J.; Yang, Y.; Wang, L.; Guan, Z. *J. Polym. Eng.* **2008**, *28*, 87–100.
(16) Son, W. K.; Youk, J. H.; Lee, T. S.; Park, W. H. *Mater. Lett.* **2005**, *59*, 1571–1575.
(17) Jung, Y. H.; Kim, H. Y.; Lee, D. R.; Park, S. Y.; Khil, M. S. *Macromol. Res.* **2005**, *13*, 385–390.
(18) Lee, H. W.; Karim, M. R.; Park, J. H.; Ghim, H. D.; Choi, J. H.; Kim, K.; Deng, Y.; Yeum, J. H. *J. Appl. Polym. Sci.* **2009**, *111*, 132–140.
(19) Guerrini, L. M.; de Oliveira, M. P.; Branciforti, M. C.; Custodio, T. A.; Bretas, R. E. S. *J. Appl. Polym. Sci.* **2009**, *112*, 1680–1687.
(20) Munir, M. M.; Iskandar, F.; Khairurrijal, O. K. *Rev. Sci. Instrum.* **2009**, *80*, 026106−3.
(21) Jeun, J.-P.; Jeon, Y.-K.; Nho, Y.-C.; Kang, P.-H. *J. Ind. Chem. Eng.* **2009**, *15*, 430–433.
(22) Ding, B.; Kim, H.-Y.; Lee, S.-C.; Shao, C.-L.; Lee, D.-R.; Park, S.-J.; Kwag, G.-B.; Choi, K.-J. *J. Polym. Sci., Part B: Polym. Phys.* **2002**, *40*, 1261–1268.
(23) Ding, B.; Kimura, E.; Sato, T.; Fujita, S.; Shiratori, S. *Polymer* **2004**, *45*, 1895–1902.
(24) Huang, C. C.; Lin, C. K.; Lu, C. T.; Lou, C. W.; Chao, C. Y.; Lin, J. H. *Fibres Text. East. Eur.* **2009**, *17*, 34–37.
(25) Jeong, J. S.; Moon, J. S.; Jeon, S. Y.; Park, J. H.; Alegaonkar, P. S.; Yoo, J. B. *Thin Solid Films* **2007**, *515*, 5136–5141.
(26) Wong, K. K. H.; Zinke-Allmang, M.; Hutter, J. L.; Hrapovic, S.; Luong, J. H. T.; Wan, W. *Carbon* **2009**, *47*, 2571–2578.
(27) Kim, G.-M.; Asran, A. S.; Michler, G. H.; Simon, P.; Kim, J.-S. *Bioinspiration Biomimetics* **2008**, *3*, 046003/1−12.
(28) Bai, J.; Li, Y.; Yang, S.; Du, J.; Wang, S.; Zheng, J.; Wang, Y.; Yang, Q.; Chen, X.; Jing, X. *Solid State Commun.* **2007**, *141*, 292–295.
(29) Hong, K. H. *Polym. Eng. Sci.* **2007**, *47*, 43–49.
(30) Adanur, S.; Ascioglu, B. *J. Ind. Textiles* **2007**, *36*, 311–327.
(31) Ji, H. M.; Lee, H. W.; Karim, M. R.; Cheong, I. W.; Bae, E. A.; Kim, T. H.; Islam, M. S.; Ji, B. C.; Yeum, J. H. *Colloid Polym. Sci.* **2009**, *287*, 751–758.
(32) Ristolainen, N.; Heikkila, P.; Harlin, A.; Seppala, J. *Macromol. Mater. Eng.* **2006**, *291*, 114–122.
(33) Shao, C.; Kim, H.-Y.; Gong, J.; Ding, B.; Lee, D.-R.; Park, S.-J. *Mater. Lett.* **2003**, *57*, 1579–1584.
(34) Medeiros, E.; Mattoso, L.; Offeman, R.; Wood, D.; Orts, W. J. *Biobased Mater. Bioenergy* **2008**, *2*, 1–12.
(35) Junkasem, J.; Rujiravanit, R.; Supaphol, P. *Nanotechnology* **2006**, *17*, 4519–4528.
(36) Zoppe, J. O.; Peresin, M. S.; Habibi, Y.; Venditti, R. A.; Rojas, O. J. *ACS Appl. Mater. Interfaces* **2009**, *1*, 1996–2004.
(37) Rojas, O. J.; Montero, G.; Habibi, Y. *J. Appl. Polym. Sci.* **2009**, *113*, 927–935.
(38) Habibi, Y.; Goffin, A.-L.; Schiltz, N.; Duquesne, E.; Dubois, P.; Dufresne, A. *J. Mater. Chem.* **2008**, *18*, 5002–5010.
(39) Habibi, Y.; Hoeger, I.; Kelley, S. S.; Rojas, O. J. *Langmuir* **2009**, DOI: 10.1021/la902444x.
(40) Azizi Samir, M. A. S.; Alloin, F.; Sanchez, J.-Y.; Dufresne, A. *Polymer* **2004**, *45*, 4149–4157.
(41) Azizi Samir, M. A. S.; Alloin, F.; Sanchez, J.-Y.; El Kissi, N.; Dufresne, A. *Macromolecules* **2004**, *37*, 1386–1393.
(42) Cao, X.; Habibi, Y.; Lucia, L. A. *J. Mater. Chem.* **2009**, *19*, 7137–7145.
(43) Young, M. L.; Su, H. K.; Seon, J. K. *Polymer* **1996**, *37*, 5897–5905.
(44) Miya, M.; Iwamoto, R.; Mima, S. *J. Polym. Sci., Polym. Phys.* **1984**, *22*, 1149–1151.
(45) Gilman, J. W.; VanderHart, D. L.; Kashiwagi, T. Thermal decomposition chemistry of poly(vinyl alcohol). Char characterization and reactions with bismaleimides. In *Fire and Polymers II: Materials and Tests for Hazard Prevention*; Nelson, G. L., Ed.; ACS Symposium Series 599; American Chemical Society: Washington, DC, 1995; pp 161−85.
(46) Fernández, M. D.; Fernández, M. J. *J. Therm. Anal. Calorim.* **2008**, *92*, 829–837.
(47) Roohani, M.; Habibi, Y.; Belgacem, N. M.; Ebrahim, G.; Karimi, A. N.; Dufresne, A. *Eur. Polym. J.* **2008**, *44*, 2489–2498.
(48) Pyda, M. ATHAS database, http://athas.prz.edu.pl/ (accessed 2009).

BM901254N